

MAPPING FLUX TRAPPING IN SRF CAVITIES TO ANALYZE THE IMPACT OF GEOMETRY

F. Kramer *, J. Knobloch, O. Kugeler, J.-M. Köszezi, Helmholtz Zentrum Berlin, Germany

Abstract

A combined temperature and magnetic field mapping system was used to investigate the impact of an ambient field on trapped flux and on the resulting local surface resistance. For this, a 1.3 GHz TESLA single cell cavity was cooled through the superconducting transition at different magnetic field angles with respect to the cavity axis. The measurements suggest, that the field is trapped homogeneously over the cavity volume, without changing its orientation. Flux trapped perpendicular the surface contributed significantly more to the surface resistance, than trapped flux parallel to the surface.

INTRODUCTION

With increasing quality standards for superconducting cavities, losses due to trapped flux must be considered, to push the cavities to their limits. Since the complete shielding of the earth's and other stray magnetic fields is impossible, research is going into understanding how magnetic flux lines are being trapped and how they increase the surface resistance.

For this purpose a combined temperature and magnetic field mapping system was designed. This setup allows to measure the temperature of the outer cavity wall of a 1.3 GHz TESLA single cell cavity in form of a heatmap and the magnetic field surrounding the cavity in 3D at 20 positions. With the aid of three Helmholtz coil pairs a magnetic field with different orientations was applied while the cavity was cycled through its transition temperature several times.

The field measured with the magnetic field sensors suggest that the magnetic flux is trapped in the cavity homogeneously and does not change its orientation because of the cavities geometry. For each orientation of the externally applied magnetic field, a Q vs E curve was taken at different temperatures so the average residual resistance could be calculated. Here an increase of the residual resistance was observed when the field was applied parallel to the beam axis as opposed to when the field was applied perpendicular to it. Furthermore the recorded heatmaps were used to calculate the local surface resistance caused by the trapped flux. Here the largest increase in surface resistance was observed when the trapped flux was perpendicular to the cavity surface.

EXPERIMENTAL SETUP

The experiment was performed in a vertical test stand with magnetic shielding to reduce the ambient field below $1 \mu\text{T}$. The investigated cavity is a 1.3 GHz TESLA single cell cavity fabricated from fine grain niobium.

* f.kramer@helmholtz-berlin.de

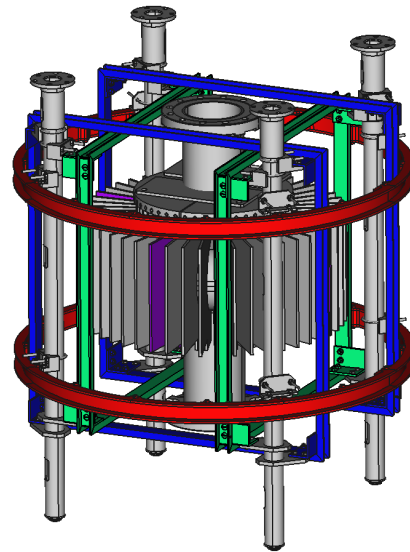


Figure 1: CAD rendering of the measurement setup. It consists of the cavity in the middle, circuit boards for measuring the temperature and B-field around it and three Helmholtz coils. The red coil generates the field in z direction, the blue in x direction and the green in y direction. The boards for measuring the magnetic field are highlighted purple, but in this depiction only two of four are visible. All other boards were used to map the temperature.

Figure 1 shows a 3D rendering of the combined temperature and magnetic field mapping system. The cavity in the middle is surrounded by up to 48 circuit boards that contain either temperature sensors or magnetic field sensors. The last experiment was performed with four boards for magnetic field measurements. They were spaced 90° apart and in line with the Helmholtz coils. In Fig. 1 they are marked purple. On the boards are 5 sensor groups consisting of 3 sensors each, so the magnetic field can be measured in 3D. The used sensors are AMR sensors AFF755B from Sensitec. [1]. The boards are described in more detail in [2].

The other available slots were used for temperature mapping cards as far as possible. The cards have either 19 or 13 100Ω carbon Allen-Bradley resistors on them that are pressed against the cavity with springs. As their resistance is highly temperature dependent at cryogenic temperatures, the resistance can be measured and used to calculate the temperature [3]. The cards with 13 and 19 sensors are alternated around the cavity, since the cavity gets narrower towards the irises and only boards with 19 sensors would not fit.

The voltage drop over the resistors and the output voltage of the AMR sensors are measured with five imc SPARTAN voltmeters with 128 channels each.

Around the cavity and circuit boards three Helmholtz coil pairs are mounted. They can be used to apply a magnetic field in an arbitrary direction. They are also described in more detail in [2]. For the experiment the cavity was cycled through its transition temperature several times. First a baseline measurement was performed where no magnetic field was applied during the phase transition. After that a B-field of $10\ \mu\text{T}$ was applied with different orientations with respect to the cavity. The polar angle α was swept from 0° (perpendicular to beam axis) to 90° (parallel to beam axis) in 15° steps. The azimuthal angle ϕ was also changed 90° once with $\alpha = 0^\circ$. The used coordinate system is depicted in Fig. 2.

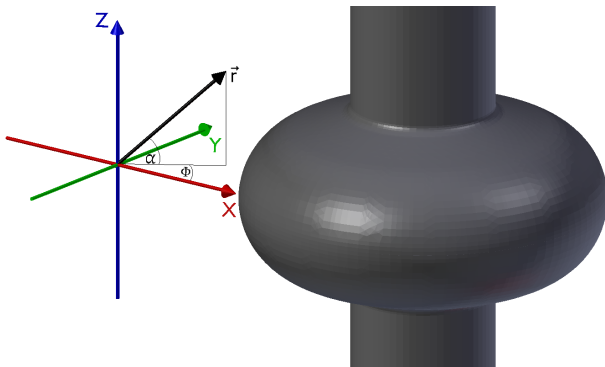


Figure 2: Used coordinate system.

EXPERIMENTAL FINDINGS

Since there was no absolute calibration of the AMR sensors possible all shown magnetic field data is not absolute but relative. As a calibration point the field configuration with the cavity in a superconducting state but without any applied field was chosen. This point was taken during the baseline measurement once the cavity was superconducting. The output voltages from the AMR sensors at that time were then said to correspond to 0 magnetic field. Consequently all measured trapped flux corresponds only to the additional trapped flux due to the Helmholtz coils and not all trapped flux, including the background.

How the Flux is Trapped

First the distribution of the magnetic field surrounding the cavity before and after the phase transition from normal to superconducting will be presented. In this example the field was applied with $\alpha = 90^\circ$.

Figure 3 shows the magnetic field when the cavity is still in a normal conducting state. The Helmholtz coils were turned on. The blue arrow indicates the orientation of the magnetic field during phase transition. However, it is not to scale. The red arrows show the magnetic field measured by the AMR sensors and the numbers next to them indicate the magnitude of the measured field.

Figure 4 shows the cavity in a superconducting state while the Helmholtz coil is still turned on. Here it can already be seen that the field orientation and magnitude only changed

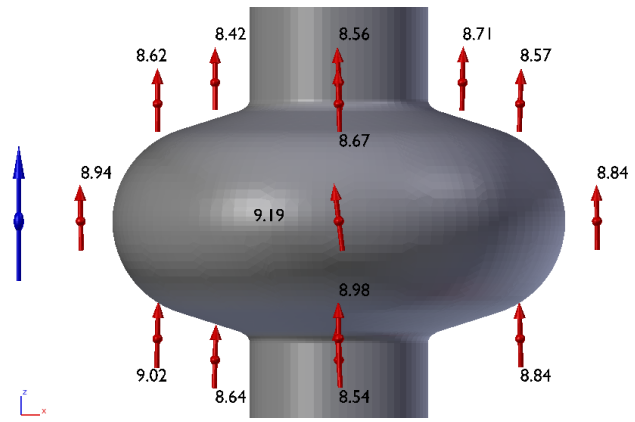


Figure 3: Measured magnetic flux density before phase transition from normal to superconducting with an applied magnetic flux density of $10\ \mu\text{T}$ in z direction. The numbers show the magnitude of the flux density in μT . The blue arrow indicates the direction of the applied external field during the phase transition. However, it is not to scale.

very slightly compared to Fig. 3. This indicates that most of the flux got trapped during the phase transition.

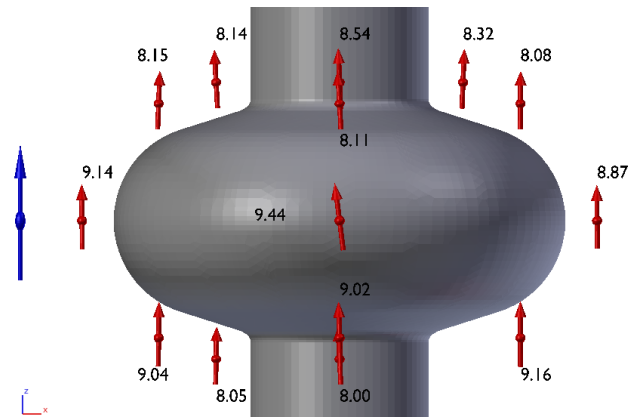


Figure 4: Measured magnetic flux density after phase transition from normal to superconducting with an applied magnetic flux density of $10\ \mu\text{T}$ in z direction. The numbers show the magnitude of the flux density in μT . The blue arrow indicates the direction of the applied external field during the phase transition. However, it is not to scale.

Figure 5 shows the cavity again in a superconducting state, but now the Helmholtz coils are turned off. This way only the flux trapped inside the cavity is measured.

In order to investigate what configuration of trapped flux would lead to the field measured at the sensor positions simulations were performed. The result of a simulation is shown in Fig. 6. Here a remanent flux density of $10\ \mu\text{T}$ with $\alpha = 90^\circ$ was set in the cavity walls. With that two assumptions are being made: First that the flux gets trapped homogeneously across the material and second that it gets trapped in the direction the external field was applied. The μ_r of the material was set to 0.0001 to represent the cavity in its superconducting state. The slice through the cavity shows

Content from this work may be used under the terms of the CC BY 3.0 licence (© 2019). Any distribution of this work must maintain attribution to the author(s), title of the work, publisher, and DOI.

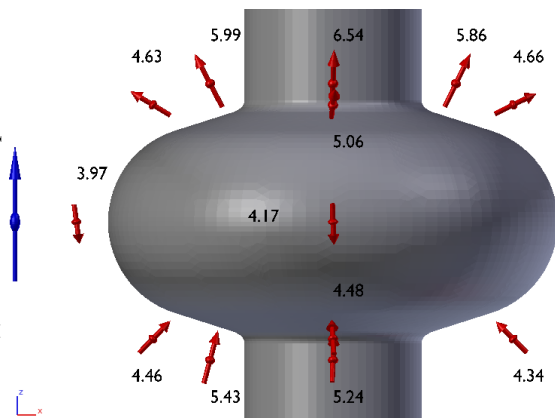


Figure 5: Measured magnetic flux density after phase transition from normal to superconducting with an applied magnetic flux density of $10\ \mu\text{T}$ in z direction. During these measurements the Helmholtz coil was turned off. The numbers show the magnitude of the flux density in μT . The blue arrow indicates the direction of the applied external field during the phase transition. However, it is not to scale.

how the flux lines close around the superconducting cavity creating a field very similar to the one in Fig. 5.

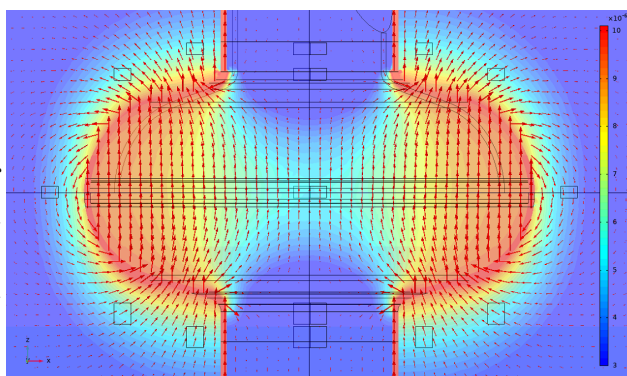


Figure 6: Simulated slice through the cavity. A remanent B-field of $10\ \mu\text{T}$ in z direction is set in the cavity walls. The black squares around the cavity indicate the sensor positions. As the lower two groups are spread further apart the squares are bigger.

To be able to compare the simulations with the measurement results the field data from the simulation was taken at the real sensor positions, indicated by the black rectangles in Fig.6. The extracted data was then visualized in the same way the measured data was. Figure 7 shows the visualization of the simulated data.

By comparing Fig. 5 and Fig. 7 the similarities become apparent. This suggests that the flux is being trapped homogeneously and without reorientation in the niobium. One difference is the relation between the magnitude of the upper two sensor groups. This is likely caused by the fact, that the cavity is cooled from the bottom to the top. Consequently the phase front moves up the cavity. The niobium under the phase front is superconducting and expels some of the

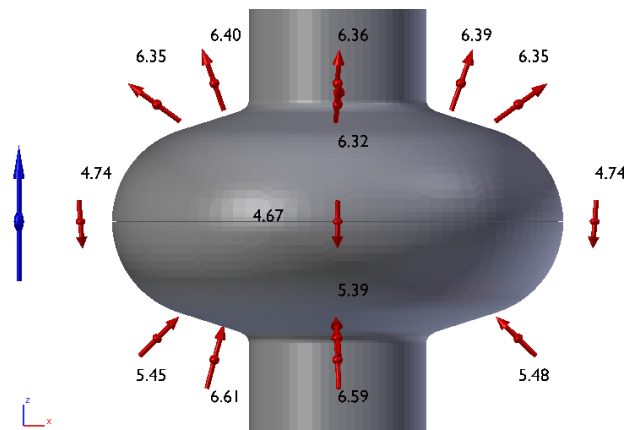


Figure 7: Simulated trapped flux at sensor positions. The external field was applied in z direction. The data was taken from the same simulation as in Fig. 6. It shows a good agreement to Fig. 5.

applied field. So when the phase front reaches the upper half of the cavity the surrounding field is already distorted, since the lower half expelled some of the flux.

Amount of Trapped Flux

With the data recorded by the AMR sensors an estimation of how much flux is being trapped is possible as well. However, since there was no absolute calibration possible and there are still some errors on the circuit boards the results have to be treated with care. But with the assumption of perfectly working AMR sensors one can use the quotient of the magnitude of measured and simulated flux densities to estimate the amount of trapped flux. Table 1 shows the averaged quotient over all sensor groups.

Table 1: Estimated Trapped Flux by Comparison with Simulations for Different Angles of the Applied Field

$\alpha[\text{deg}]$	$\langle \vec{B}_{\text{meas}} / \vec{B}_{\text{sim}} \rangle [\%]$
0	66 ± 2
15	52 ± 3
30	80 ± 12
45	76 ± 1.3
75	71 ± 6
90	88 ± 3

Here a trend is visible that more flux is trapped when the field is applied parallel to the beam axis. However, this effect is probably amplified by a systematic error of the AMR sensors during the measurements.

Another way to estimate the amount of trapped flux is to investigate the amount of expelled flux: When 100% of the applied field gets trapped, the phase transition is not visible on the magnetic field sensors, since the field configuration does not change. When all flux gets expelled and 0% gets trapped, the transition is very clear, as the flux gets pushed out the cavity and in some sensor positions the flux density

increases and in other the flux density decreases. In the real experiment only a fraction of the flux gets trapped and the change in flux density is in between the two extreme cases. As a first approximation a linear interpolation between the extreme cases was performed and compared with the data of a cooldown.

The data for the case of 100% trapping was taken from Fig. 3 when the cavity was still normal conducting (B_n). The case of 0% trapping is shown in Fig. 8. This data was taken after the baseline measurement where the cavity was cooled down without any applied field. While the cavity was still superconducting a magnetic field was applied. This mimics full expulsion (B_{fe}). However, data of this kind is only available for $\alpha = 90^\circ$ and $\alpha = 0^\circ$. To calculate the fraction q of trapped flux, the following equation was used

$$q = 1 - \frac{B_n - B_{tf}}{B_n - B_{fe}} \quad (1)$$

With the measured flux density B_{tf} when flux was trapped partially. The results are shown in Table 2. This method also shows less flux being trapped when the field is applied perpendicular to the beam axis.

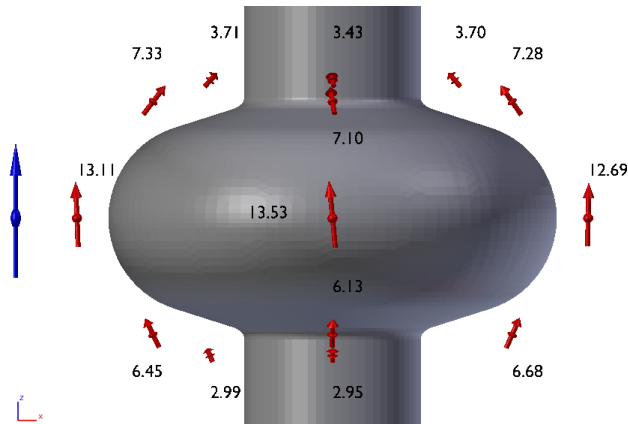


Figure 8: As the Helmholtz coil was turned on after the cavity was superconducting, this state mimics full expulsion. The field was applied in z direction ($\alpha=90^\circ$).

Table 2: Estimated Trapped Flux by Interpolating Linearly between 0% and 100% Trapping

α [deg]	$\langle q \rangle$ [%]
0	81 ± 2
90	93 ± 4

Average Surface Resistance

For each applied field a systematic quality factor measurement was carried out. So the quality factor was measured at accelerating fields of 2.5, 5, 7.5, 10, 12.5, 15, 17.5 MV/m at 1.51, 1.61, 1.72, 1.8, 1.86 K. Higher fields were left out on purpose, since the risk of quenching the cavity would get too high. Once the cavity quenched the trapped flux would

have the chance to redistribute or even leave the cavity, depending on the size and position of the quench. The surface resistance R_s can be calculated via $R_s = G/Q_0$. Here G is the geometry factor which is 250Ω for single cell TESLA cavity [4]. By using

$$R_s = \left(\frac{af^2}{T} \right) \exp\left(-\frac{bT_c}{T} \right) + R_{res} \quad (2)$$

the residual resistance R_{res} could be extracted from the surface resistance. a and b are fit parameters which depend on material properties, f is the RF frequency, T is the cavity's temperature and T_c is the critical temperature of niobium [5].

The results of the fit for 5 MV/m are shown in Fig. 9 where a dependency on the polar angle of the applied field is visible.

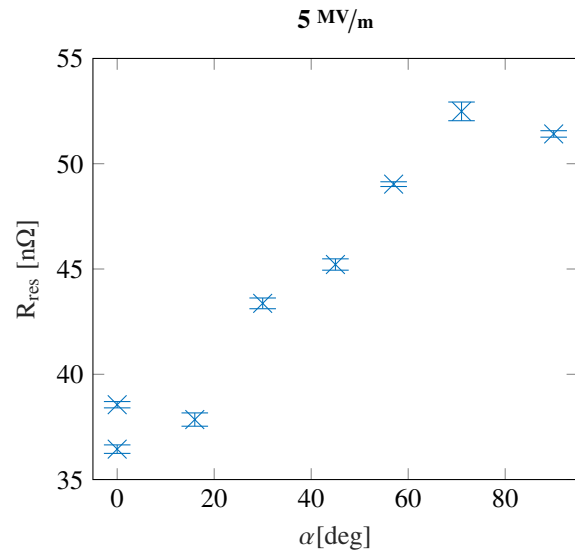


Figure 9: Scaled R_{res} vs. α for 5 MV/m. There are two points at 0° , because for both applied field in x and y direction α equals zero. The residual resistance for the x direction is higher.

Local Surface Resistance

Figure 10 shows the heatmap of the baseline measurement when no external field was applied during cooldown. It shows more or less even heating of the cavity surface.

Figure 11 shows the relative heating of the cavity when the external magnetic field was applied in x direction ($\alpha = 0^\circ, \phi = 0^\circ$). Relative heating means that the heatmap recorded during the baseline measurement without any externally applied field (Fig. 10) is subtracted from the heatmap recorded when there was a field present during cooldown. In this representation the field is perpendicular to the cavity surface at $\phi = 352.5^\circ$ and $\phi = 172.5^\circ$ at equator level. At these positions the cavity heats up more.

The heatmaps can also be used to calculate the local surface resistance. This is done in the following way: The quality factor of the baseline measurement was used to calculate the average surface resistance of the cavity with no

Content from this work may be used under the terms of the CC BY 3.0 licence under the terms of the CC BY 3.0 licence (© 2019). Any distribution of this work must maintain attribution to the author(s), title of the work, publisher, and DOI.

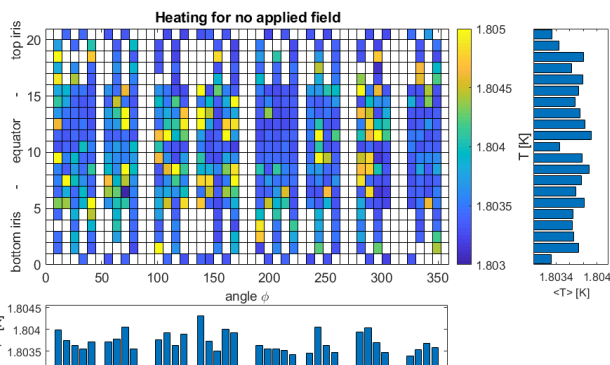


Figure 10: Heatmap of baseline measurement without any applied external field. The bar plots show the average temperature for a column or row respectively.

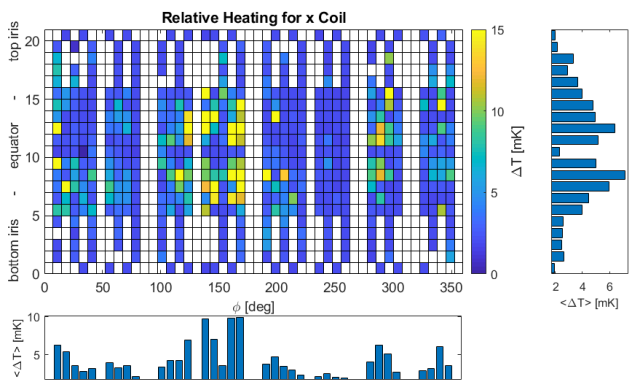


Figure 11: Relative heating for applied field in x direction. The externally applied magnetic field is perpendicular to the cavity surface at $\phi = 352.5^\circ$ and $\phi = 172.5^\circ$ at equator level. The bar plots show the average temperature rise for a column or row respectively.

applied field with $R_s = G/Q_0$ and $G = 250 \Omega$ [4]. Assuming a homogeneous surface resistance allows to calibrate the thermal connection of the sensors:

The surface resistance is proportional to the rise of temperature ΔT when the RF field is turned on. It is also inversely proportional to the square of the RF magnetic field H^2 . For every sensor a calibration constant ξ_i can be introduced, so the measured temperature rise of this sensor ΔT_i corresponds to the mean surface resistance R_s .

$$R_s = \frac{\xi_i \Delta T_i}{H^2} \Leftrightarrow \xi_i = \frac{R_s H^2}{\Delta T_i} \quad (3)$$

Of course the surface resistance is not perfectly homogeneous across the cavity, even when no field is applied. But this spread is an order of magnitude smaller than the differences observed when an external field was applied.

In the following calculations, only the middle part (row 5 to 15) of the heatmaps were taken into account. As there is a more consistent coverage of the surface with temperature sensors. Also the RF magnetic field only has a deviation of 5% over this area. In order to get a more even and realistic heatmap, the temperature points were averaged with the four

surrounding points. That was done by weighing the point itself times four and the surrounding sensors times one. If the sensor was on an edge, it was only averaged with the remaining two or three neighbours. Figure 12 shows the resulting local surface resistance. Here a clear dependency on the azimuthal angle ϕ is visible in the bar chart.

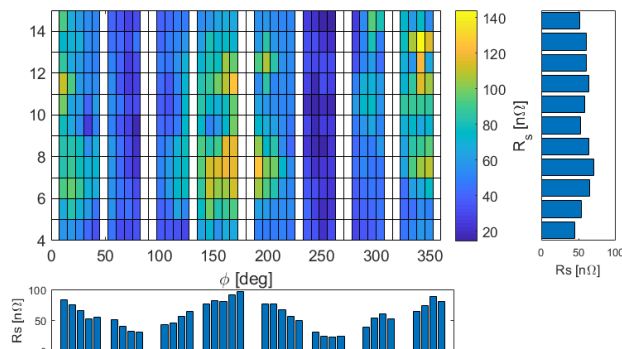


Figure 12: Calculated local surface resistance, with applied field in x direction. Only the middle section of the heatmap was used (row 5-15).

Figure 13 shows the surface resistance versus the azimuthal angle ϕ extracted from Fig. 12. Since the B-field perpendicular to the surface is suspected to cause the highest increase in surface resistance, $|\cos(\phi)|$ is also shown the plot. It is the absolute of the cosine, because in this model it does not matter, whether the frozen flux points in or out of the surface. It is shifted 7.5° to the left, as the field is perpendicular at 352.5° and 172.5° instead of 0° and 180° . It is also scaled up and shifted upwards, to fit the data points. The resulting equation is $y = (65 \cdot |\cos(\phi + 7.5)| + 22) \text{n}\Omega$

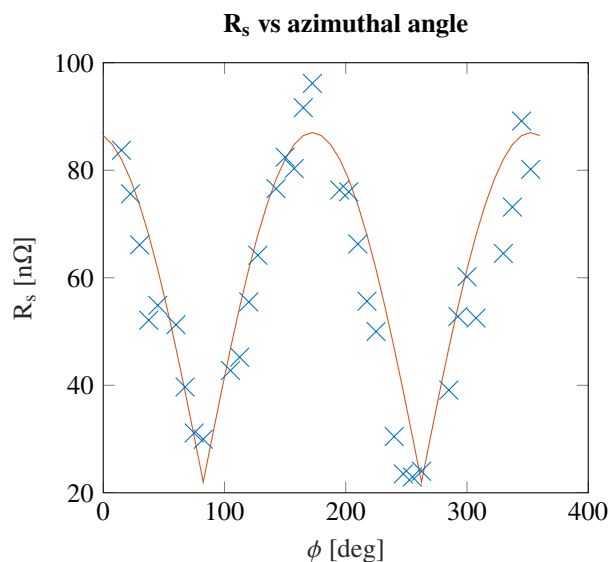


Figure 13: Calculated surface resistance vs azimuthal angle with applied field in x direction. The blue marks show the averaged columns from Figure 12. The red graph follows $y = (65 \cdot |\cos(\phi + 7.5)| + 22) \text{n}\Omega$

The plot in Figure 13 again supports the statement, that the surface perpendicular to the B-field creates the largest contribution to the surface resistance, as the resistance follows the $|\cos|$.

Figure 14 and Fig. 15 show the averaged surface resistance of the columns and rows for applied field in z direction respectively.

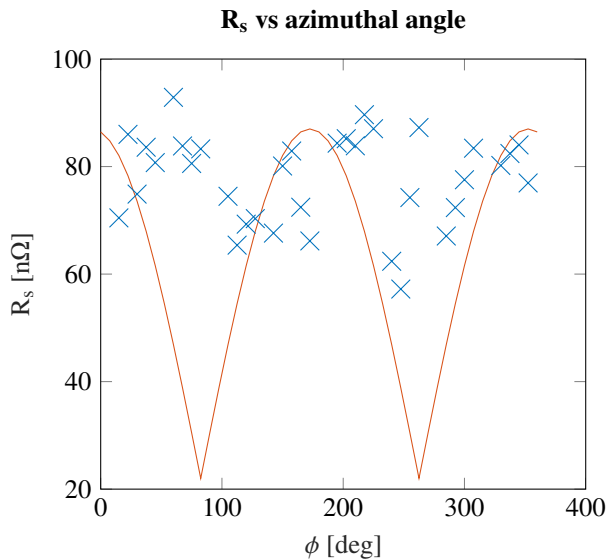


Figure 14: Calculated surface resistance vs azimuthal angle with applied field in z direction. The blue marks show the averaged surface resistance. The red graph follows $y = (65 \cdot |\cos(\phi + 7.5)| + 22)\text{n}\Omega$. It visualizes the difference between these results and the ones in Fig. 13.

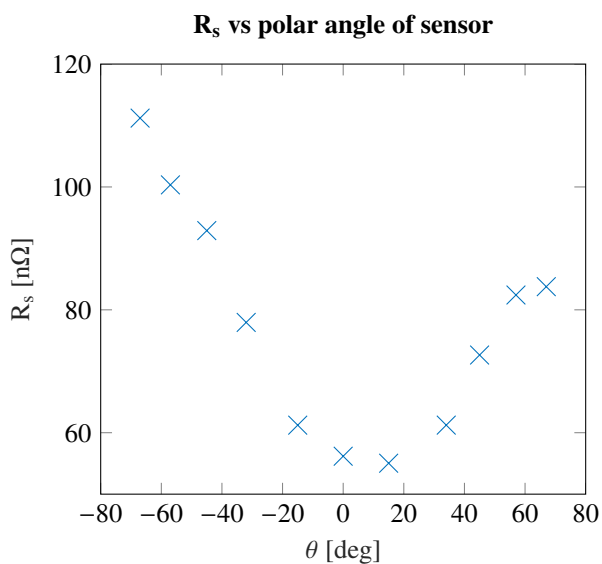


Figure 15: Calculated surface resistance vs polar angle, with applied field in z direction. The polar angle is defined the same as before. So 0° is at the equator. The blue marks show the averaged surface resistance.

The plots in Fig. 14 and Fig. 15 show the expected result. There is no dependency on the azimuthal angle. The dependency on the polar angle also shows that at the equator the surface resistance is at its minimum. Here the field is parallel to the surface. The top bottom asymmetry shown earlier in the results of the magnetic field mapping is also visible.

SUMMARY AND OUTLOOK

With the three dimensional magnetic mapping system it was possible to resolve and visualize the magnetic field surrounding a superconducting cavity for the first time. With this data a statement could be made, about how the magnetic field is trapped. Comparing the measured data to results from simulations suggests that the field gets trapped homogeneously over the cavity volume without any reorientation of the flux lines, regardless of the applied field angle.

On the heatmaps moving hotspots were observed depending on the direction of the applied field. By calibrating the sensors with a baseline measurement, the local surface resistance could be calculated. The results showed a bigger increase of surface resistance where the field was perpendicular to the surface and a smaller increase where it was parallel.

In the future similar experiments with different materials can be performed to investigate the flux expulsion of those materials and how the trapped flux influences their surface resistance. The next test is planned with a cavity fabricated from large grain niobium, to examine the influence of the grain structure on flux trapping.

Also dynamic processes can be studied with the setup. This means flux expulsion while the phase front is moving up the cavity can be investigated. Quench studies can be carried out as well where the redistribution of the trapped flux during a quench can be observed.

REFERENCES

- [1] "Aff755b magnetoresistive field sensor", Sensitec GmbH, 2018.
- [2] B. Schmitz, "Ortsauflösende Magnetometrie zur Untersuchung von eingefrorenem Magnetfluss in supraleitenden HF Kavitäten", Master's thesis, Universität Siegen, 2017.
- [3] J. Knobloch, "Advanced thermometry studies of superconducting radio-frequency cavities", Dissertation, Cornell University, 1997.
- [4] P. Bauer, A.-M. Valente-Feliciano, G. Ciovati, J. Halbritter, B. Visentin, C. Antoine, S. Calatroni, A. Gurevich, J. Knobloch, "Review of models of rf surface resistance in high gradient niobium cavities for particle accelerators", Technical Report TD-04-014, 2004.
- [5] J.-M. Köszegei, "Surface resistance minimization in srf cavities by reduction of thermocurrents and trapped flux", Dissertation, Universität Siegen, 2016.